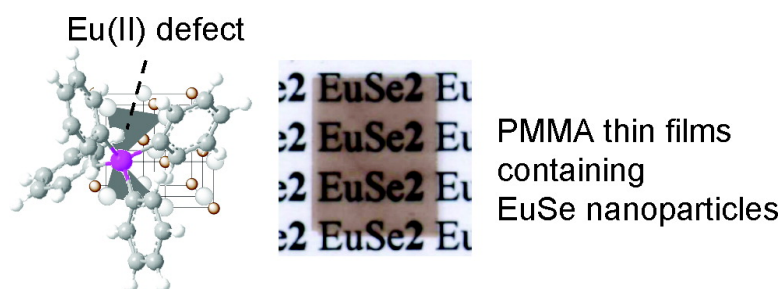Article

Remarkable Magneto-Optical Properties of Europium Selenide Nanoparticles with Wide Energy Gaps

Yasuchika Hasegawa, Taka-aki Adachi, Atsushi Tanaka, Mohammad Afzaal, Paul O'Brien, Takahiro Doi, Yukio Hinatsu, Koji Fujita, Katsuhisa Tanaka, and Tsuyoshi Kawai

Eu(II) defect

PMMA thin films containing EuSe nanoparticles

More About This Article

Additional resources and features associated with this article are available within the HTML version:

- Supporting Information
- Access to high resolution figures
- Links to articles and content related to this article
- Copyright permission to reproduce figures and/or text from this article

View the Full Text HTML

Remarkable Magneto-Optical Properties of Europium Selenide Nanoparticles with Wide Energy Gaps

Yasuchika Hasegawa,[†,*] Taka-aki Adachi,[†] Atsushi Tanaka,[†] Mohammad Afzaal,[‡] Paul O'Brien,[‡] Takahiro Doi,[§] Yukio Hinatsu,[§] Koji Fujita,[¶] Katsuhisa Tanaka,[¶] and Tsuyoshi Kawai[†,*]

Graduate School of Materials Science, Nara Institute of Science and Technology, 8916-5 Takayama-cho, Ikoma, Nara 630-0192, Japan, The School of Chemistry and The School of Materials, The University of Manchester, Oxford Road, Manchester M13, 9PL, U.K., Graduate School of Science, Hokkaido University, North 10 West 8, Sapporo, Hokkaido 060-0810, Japan, and Department of Material Chemistry, Graduate School of Engineering, Kyoto University, Katsura, Nishikyo-ku, Kyoto 615-8510, Japan

Received November 8, 2007; E-mail: hasegawa@ms.naist.jp; tkawai@ms.naist.jp

Abstract: The enhanced magneto-optical properties of nanoscaled lanthanide chalcogenide semiconductors which have a wide energy gap were observed at around 500 nm for the first time. The nanoscaled semiconductors, $Eu_{1-x}Se$ nanoparticles **1** (cubic shapes) and **2** (spherical shapes), were synthesized by the thermal reduction of Eu(III) ion with organic ligands containing Se atoms. The resulting $Eu_{1-x}Se$ nanoparticles were characterized by X-ray diffraction, high-resolution transmission electron microscopy, energy dispersive X-ray spectroscopy, superconducting quantum interference devices magnetometer, and microwave induced plasma atomic emission spectroscopy measurements. The particle grain sizes of **1** and **2** were estimated to be 11 and 20 nm, respectively. The concentration-normalized Veldet constants (the magnitude of the Faraday effect) of $Eu_{1-x}Se$ nanoparticles were much larger than those of corresponding bulk EuSe and EuS nanoparticles.

Introduction

There has been considerable current interest in the synthesis of semiconductor nanocrystals as nanoscale powders dispersible in aqueous or nonaqueous media. Such materials have potential applications including use in displays, biological tagging materials, next generation photovoltaics, and lasers.[1–7] The optical properties of semiconductor nanoparticles are dominated by their band gaps and their electronic structure related to size, shape, and the environments surrounding the particles.[8] Additional

functionality can be introduced by combining their optical and magnetic effects, and certain lanthanide chalcogenides are particularly attractive in this respect. Lanthanide chalcogenides, especially the europium chalcogenides (EuO, EuS, EuSe, and EuTe) were intensely studied in the 1970s[9] and continue to be of both theoretical[10] and experimental[11] interest. Europium chalcogenide semiconductors are characterized by narrow 4f orbitals that exist as degenerate levels between the conduction band (5d orbitals of Eu(II)) and the valence band (p orbitals of O^{2-}, S^{2-}, Se^-, or Te^{2-}).[9] The 4f–5d electronic transition and

[†] Nara Institute of Science and Technology.
[‡] The University of Manchester.
[§] Hokkaido University.
[¶] Kyoto University.
(1) Tessler, N.; Medvedev, V.; Kazes, M.; Kan, S.; Banin, U. *Science* **2002**, *295*, 1506.
(2) Coe, S.; Woo, W.; Bawendi, M. G.; Bulovic, V. *Nature* **2002**, *420*, 800.
(3) Bruchez, M., Jr.; Moronne, M.; Gin, P.; Weiss, S.; Alivisatos, A. P. *Science* **1998**, *281*, 2013.
(4) Huynh, W. U.; Dittmer, J. J.; Alivisatos, A. P. *Science* **2002**, *295*, 2425.
(5) Klimov, V. I.; Mikhailovsky, A. A.; Xu, S.; Malko, A.; Hollingsworth, J. A.; Leatherdale, C. A.; Eiler, H.-J.; Bawendi, M. G. *Science* **2000**, *290*, 314.
(6) Trindade, T.; Pickett, N. L.; O'Brien, P. *Chem. Mater.* **2001**, *13*, 3843.
(7) Pickett, N. L.; O'Brien, P. *Chem. Record* **2001**, *1*, 467.
(8) Recent paper on nanoparticles: Urban, J. J.; Talapin, D. V.; Shevchenko, E. V.; Kagan, C. R.; Murray, C. B. *Nat. Mater.* **2007**, *6*, 115. (b) Protasenko, V.; Bacinello, D.; Kuno, M. *J. Phys. Chem. B* **2006**, *110*, 25322. (c) Shanbhag, S.; Kotov, N. A. *J. Phys. Chem. B* **2006**, *110*, 12211. (d) Shevchenko, E. V.; Talapin, D. V.; Murray, C. B.; O'Brien, S. *J. Am. Chem. Soc.* **2006**, *128*, 3620. (d) Shevchenko, E. V.; Talapin, D. V.; Kotov, N. A.; O'Brien, S.; Murray, C. B. *Nature* **2006**, *439*,

(55) (e) Gattas-Asfura, K. M.; Constantine, C. A.; Lynn, M. J.; Thimann, D. A.; Ji, X. J.; Leblanc, R. M. *J. Am. Chem. Soc.* **2005**, *127*, 14640. (f) Chan, Y.; Zimmer, J. P.; Stroh, M.; Steckel, J. S.; Jain, R. K.; Bawendi, M. G. *Adv. Mater.* **2004**, *16*, 2092. (g) Talapin, D. V.; Mekis, I.; Goetzinger, S.; Kornowski, A.; Benson, O.; Weller, H. J. *J. Phys. Chem. B* **2004**, *108*, 18826. (h) Wang, Y.; Tang, Z.; Correa-Duarte, M. A.; Pastoriza-Santos, I.; Giersig, M.; Kotov, N. A.; Liz-Marzan, L. M. *J. Phys. Chem. B* **2004**, *108*, 15461. (i) Gu, F.; Wang, S. F.; Lue, M. K.; Zhou, G. J.; Xu, D.; Yuan, D. R. *J. Phys. Chem. B* **2004**, *108*, 8119. (j) Shavel, A.; Gaponik, N.; Eychmueller, A. *J. Phys. Chem. B* **2004**, *108*, 5905. (k) Wei, S.; Lu, J.; Yu, W.; Qian, Y. *J. Appl. Phys.* **2004**, *95*, 3683. (l) Borchert, H.; Talapin, D. V.; Gaponik, N.; McGinley, C.; Adam, S.; Lobo, A.; Moeller, T.; Weller, H. *J. Phys. Chem. B* **2003**, *107*, 9662.
(9) Wachter, P. *Handbook on the Physics and Chemistry of Rare Earth*, 2nd ed.; CRC Critical Reviews in Solid State Science; North-Holland Publishing Company: 1979; p 189.
(10) (a) Ariponnammal, S.; Natarajan, S. *Mod. Phys. Lett. B* **2000**, *14* (24), 843–848. (b) Kunes, J.; Ku, W.; Pickett, W. E. *J. Phys. Soc. Jpn.* **2005**, *74* (5), 1408.
(11) (a) Sakalle, U. K.; Jha, P. K.; Sanyal, S. P. *Bull. Mater. Sci.* **2000**, *23* (3), 233–235. (b) Kasuya, T. *J. Magn. Magn. Mater.* **1999**, *195* (1), 141–147. (c) Gorlitz, D.; Kotzler, J. *Eur. Phys. J., B* **1998**, *5* (1), 37–43.

spin configuration of europium(II) chalcogenides lead to large Faraday and Kerr effects,[12] making them promising candidates as active materials in magneto-optic devices.

Recently, europium oxide and sulfide nanoparticles have been synthesized, and their resulting magneto-optical properties have been explored.[13] Gao and Stoll have studied the magnetic properties of europium(II) sulfide (EuS) nanoparticles.[14] Although the magnetic properties of the europium(II) chalcogenide nanoparticles with smaller diameters than the magnetic correlation distance are considerably weaker than bulk counterparts, their magneto-optical properties are improved because of confined electronic states and enhanced optical transition cross-section. The magneto-optical properties of europium chalcogenide nanoparticles are strongly dependent on their size, shape, and surface environments.[15] Recently, we have reported on the manipulation of Faraday rotation wavelength between 580 and 640 nm (red-light region) by using size-controlled EuS nanoparticles (particle size: 7−14 nm).[16] The europium(II) chalcogenide nanoparticles which have shorter resonance wavelengthes than 550 nm are expected to be useful in applications such as optical isolator and magneto-optical memory using green and blue laser lights. Smaller EuS nanoparticles (size <6 nm) would lead to a significant blue shift of the Faraday rotation wavelength; however, the magnitude of the magneto-optical effect (the Veldet constant on the Faraday rotation) might be reduced owing to their decreased magnetic susceptibility.[17] Effective Faraday rotation wavelength at around 500 nm requires that novel europium chalcogenide nanoparticles should have a larger energy gap of 4f−5d transition.

Here, we focus on EuSe nanoparticles that have a wide energy gap as a novel magneto-optical material. It is known that the energy gap of bulk EuSe (1.80 eV) is wider than that of EuS (1.65 eV).[9,18] The wide energy gap of EuSe nanoparticles would lead to an effective magneto-optical property at around 500 nm. Furthermore, the ferromagnetic coupling in the bulk EuSe is not only confined to a single (111) plane, but extends to over neighboring (111) planes. Their wide ferromagnetic coupling has been attributed to the NNSS-spin structure.[9]

In the present study, we initially report the synthesis of EuSe nanoparticles with Eu defects ($Eu_{1-x}Se$) followed by their remarkable magneto-optical properties in the shorter active wavelength than 600 nm. The preparation of $Eu_{1-x}Se$ nanoparticles are carried out by the thermal reduction of Eu(III)
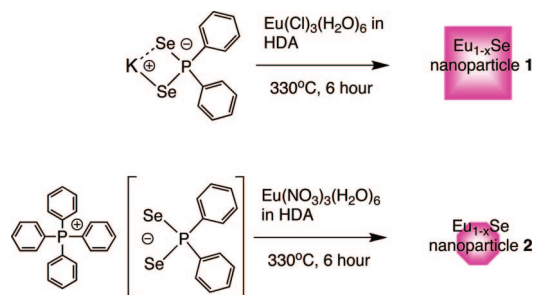

Figure 1. Reaction schemes of $Eu_{1-x}Se$ nanoparticles **1** and **2**.

complexes containing diphenyldiselenophosphinate ligands: $(C_6H_5)_2PSe_2$, in 1-hexadecylamine (HDA) at 300 °C (Figure 1, $Eu_{1-x}Se$ nanoparticles **1**). In subsequent experiment, $Eu_{1-x}Se$ nanoparticles containing tetraphenylphoshine cations (Figure 1, $Eu_{1-x}Se$ nanoparticles **2**) are also prepared and the influence of cationic species on the $Eu_{1-x}Se$ surface is discussed.[19] The $Eu_{1-x}Se$ nanoparticles were characterized by XRD, TEM (high-resolution transmission electron microscopy), EDX (energy dispersive X-ray spectroscopy), SQUID (superconducting quantum interface device) and MIP-AES (microwave induced plasma atomic emission spectroscopy) measurements. The particle size of $Eu_{1-x}Se$ nanoparticles **1** and **2** were estimated to be 11 and 20 nm, respectively. We successfully observed the remarkable Faraday rotation of the $Eu_{1-x}Se$ nanoparticles at around 500 nm in polymer thin films. The concentration-normalized Veldet constants of thin films containing $Eu_{1-x}Se$ nanoparticles were much larger than those of corresponding bulk EuS and $Eu_{1-x}Se$ nanoparticles as reported in the literatures (particle size: 20 nm).[15] This contribution describes the first synthesized characterization of $Eu_{1-x}Se$ nanoparticles, although a EuSe nanoisland deposited on a nanopatterned PbSe template (thickness = 50 nm) has been repoted.[20] The EuSe nanoparticles are expected to be novel magneto-optical materials in green- and blue-light regions.

Experimental Section

Materials. Europium(III) chloride hexahydrate ($EuCl_3 \cdot 6H_2O$) and europium(III) nitrate hexahydrate ($Eu(NO_3)_3 \cdot 6H_2O$) were purchased from Kanto Chemical Co. Inc. Selenium powder was purchased from Nakalai tesque. Inc. Tetraphenylphosphonium bromide ($BrPPh_4$) and polymethylmethacrylate were purchased from Wako Pure Chemical Industries Ltd. 1-Hexadecylamine (HDA) was obtained from Tokyo Chemical Industry Co., Ltd. Potassium diphenylphosphide was obtained from Aldrich Chemical Co. Inc. All other chemicals were reagent grade and were used as received.

Preparation of Potassium Diphenylphosphinediselenide $K(Se_2$-$P(C_6H_5)_2)$. Grey selenium powder (0.155 g, 2 mmol) was added to a solution of potassium diphenylphosphine in 10 mL THF (5N, 0.9 mmol) and stirred for 6 h under argon atmosphere at −30 °C. After the reaction, the mixture was filtered, and the solution was concentrated. Recrystallization from hexane gave white crystals of $K(Se_2P(C_6H_5)_2)$. Yield: 74%. ^1H NMR (CD_3SOCD_3) $\delta = 8.02$ (m, PC_6H_5 4H), 7.24 (m, PC_6H_5 6H) ppm. ^{13}C NMR (CD_3SOCD_3) $\delta = 130.87$, 130.72, 128.30, 128.25, 126.77, 126.61 ppm. ^{31}P NMR (CD_3SOCD_3) 24.02 ppm. ESI-MS: 344.88. Anal. Calcd for $C_{12}H_{10}KPSe_2 \cdot H_2O$: C, 36.01; H, 3.02%. Found: C, 36.75; H, 2.66%.

(12) Suits, J. C.; Argyle, B. E.; Freiser, M. J. *J. Appl. Phys.* **1966**, *37*, 1391.

(13) (a) Hasegawa, Y.; Thongchant, S.; Wada, Y.; Tanaka, H.; Kawai, T.; Sakata, T.; Mori, H.; Yanagida, S. *Angew. Chem., Int. Ed.* **2002**, *41*, 2073. (b) Thongchant, S.; Hasegawa, Y.; Wada, Y.; Yanagida, S. *J. Phys. Chem. B* **2003**, *107*, 2193. (c) Mirkovic, T.; Hines, M. A.; Nair, P. S.; Scholes, G. D. *Chem. Mater.* **2005**, *17*, 3451. (d) Hasegawa, Y.; Afzaal, M. A.; O'Brien, P.; Wada, Y.; Yanagida, S. *Chem. Commun.* **2005**, 242. (e) Regulacio, M. D.; Tomson, N.; Stoll, S. L. *Chem. Mater.* **2005**, *17*, 3114. (f) Redigolo, M. L.; Koktysh, D. S.; Rosenthal, S. J.; Dickerson, J. H. *Physica Status Solidi C* **2007**, *4*, 406–408.

(14) (a) Zhao, F.; Sun, H.-L.; Su, G.; Gao, S. *Small* **2006**, *2*, 244. (b) Zhao, F.; Sun, H.; Gao, S.; Su, G. *J. Mater. Chem.* **2005**, *15*, 4209. (c) Regulacio, M. D.; Bussmann, K.; Lewis, B.; Stoll, S. L. *J. Am. Chem. Soc.* **2006**, *126*, 11173.

(15) Thongchant, S.; Hasegawa, Y.; Wada, Y.; Yanagida, S. *Jpn. J. Appl. Phys* **2003**, *107*, 2193.

(16) Kataoka, T.; Tsukahara, Y.; Hasegawa, Y.; Wada, Y. *Chem. Commun.* **2005**, 6038.

(17) Thongchant, S.; Hasegawa, Y.; Wada, Y.; Yanagida, S. *Chem. Lett.* **2003**, *32*, 706.

(18) Eastman, D. E.; Holtzberg, F.; Methfessel, S. *Phys. Rev. Lett.* **1969**, *23*, 226.

(19) (a)) Hasegawa, Y.; Okada, Y.; Kataoka, K.; Sakata,T.; Mori, M.; Wada, Y. *J. Phys. Chem. B* **2006**, *110*, 9008. b) Adachi, T.; Tanaka, A.; Hasegawa, Y.; Kawai, T. *Thin Solid Films*, in press.

(20) Schülli, T. U.; Lechner, R. T.; Stangl, J.; Springholz, G.; Bauer, G.; Dhesi, S.; Bencok, P. *Appl. Phys. Lett.* **2004**, *84*, 2661.

Preparation of Tetraphenylphosphonium Diphenylphosphine-diselenide (PPh₄(Se₂P(C₆H₅)₂). A solution of $K(Se_2P(C_6H_5)_2)$ (1.54 g 4.0 mmol) in methanol was added to BrPPh₄ (1.69 g, 4.0 mmol) dissolved in methanol and stirred. After 30 min of reaction, the resulting precipitate was separated by filtration and washed several times with water. Recrystallization from hexane gave yellow crystals of (PPh₄)(Se₂P(C₆H₅)₂). Yield: 84%. ^1H NMR (CD₃SOCD₃) $\delta =$ 7.82 (m, PC₆H₅ 24H), 7.26 (m, PC₆H₅ 6H) ppm. ^{13}C NMR (CD₃SOCD₃) $\delta =$ 135.4, 134.6, 130.8, 130.5, 127.3, 126.7, 118.3, 117.1 ppm. ESI-MS: 344.78 (negative mode), 339.06 (positive mode). Anal. Calcd for C₃₆H₃₀P₂Se₂·H₂O: C, 61.72; H, 4.60%. Found: C, 62.43; H, 4.28%.

Preparation of Eu₁₋ₓSe Nanoparticles 1. Selenium powder (0.155 g 2 mmol) was added to a solution of potassium diphenylphosphine in 10 mL THF (5N, 0.9 mmol) and stirred for 6 h under argon atmosphere at −30 °C. EuCl₃6(H₂O) (0.078 g, 0.3 mmol) was added to the reaction mixture and stirred under nitrogen atmosphere for 10 min. The reaction mixture was concentrated and added to hexadecylamine (HAD: 6 g) at 330 °C under nitrogen atmosphere. After 4 h of reaction, the resulting powder was cooled to room temperature. This powder was separated by centrifugation and washed with *n*-hexane. After washing, brown powder was obtained.

Preparation of Eu₁₋ₓSe Nanoparticles 2. A solution of (PPh₄)-(Se₂P(C₆H₅)₂) (0.30 g, 0.44 mmol) in acetonitrile was added to Eu(NO₃)₃·6(H₂O) (0.20 g, 0.44 mmol) dissolved in acetonitrile and stirred under nitrogen atmosphere for 10 min. The reaction mixture was concentrated and added to hexadecylamine (HDA) at 330 °C under nitrogen atmosphere. After 4 h of reaction, the resulting powder was cooled to room temperature. This powder was separated by centrifugation and washed with *n*-hexane. After washing, brown powder was obtained.

Apparatus. ^1H NMR, ^{13}C NMR, and ^{31}P NMR data were measured by a JEOL AL-300 (300 MHz) and ECP-400 (400 MHz) spectrometer. ^1H NMR and ^{13}C NMR chemical shifts were determined by using tetramethylsilane (TMS) as an internal standard. ^{13}P NMR chemical shifts were determined using H₃PO₄ as an internal standard. Elemental analyses were performed with a Perkin-Elmer 2400II CHNS/O. MIP-MS were recorded on a HITACHI P-6000. High-resolution images of the EuSe nanoparticles were obtained with a Hitachi JEM-3100FEF TEM equipped with a tilting device (±10 degrees) and operated at 300 kV. Energy dispersive X-ray spectroscopy (EDX) was performed with a JEOL EM-Z01299TJEC. The magnetic measurements were carried out using a Quantum Design MPMS SQUID system (superconducting quantum interference devices magnetometer).

Preparation of Polymer Thin Films Containing Euse Nanoparticles and Faray Rotation Measurements. The obtained Eu₁₋ₓSe nanoparticles (20 mg) were added to a chloroform solution (1 mL) of polymethylmethacrylate (PMMA) (2.0 g) and dispersed well under ultrasonic treatment, giving the colloidal suspension. The PMMA thin films were prepared on a glass substrate from the colloidal suspension via spin-coat method (spin-coater: MAKASA 1H-D7) for Faraday rotation measurements.

The Faraday effect measurements were performed by a measurement system for Faraday and Kerr effects (JASCO, Model K-250). A Xe lamp was used as a light source. The external magnetic field was 1.5 T. The thickness of the PMMA thin films containing Eu₁₋ₓSe nanoparticles were measured by a surface profiler KLA Tencor ALPHA STEP 500.

Results and Discussion

Characterizations and Particle Growth Mechanism of Eu₁₋ₓSe Nanoparticles. The formation of crystalline HDA-capped Eu₁₋ₓSe nanocrystals is carried out in situ generated europium diselenophosphinate compounds. XRD confirmed the formation of crystalline EuSe nanocrystals (Figure 2). Diffraction peaks $2\theta = 24.5°, 28.6°, 41.0°, 48.6°, 51.0°, 59.5°, 67.4°$ and 75.0
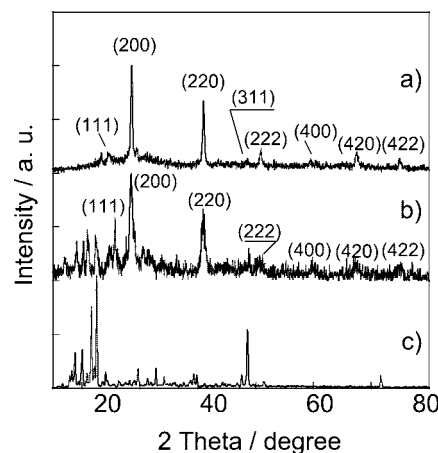

Figure 2. XRD profiles of (a) Eu₁₋ₓSe nanoparticles **1**, (b) Eu₁₋ₓSe nanoparticles **2**, and (c) (PPh₄)(Se₂P(C₆H₅)₂).

were assigned to the (111), (200), (220), (311), (222), (400), (420) and (422) planes of NaCl type EuSe, respectively. The intensity ratio of the diffraction patterns agreed with those of the bulk EuSe. We evaluated the fwhm (full width at half-maxim) of $2\theta = 28.6°$ (200), which corresponds to the Bragg diffraction using the EuSe (200) plane. The crystal grains of Eu₁₋ₓSe nanoparticles **1** and **2** calculated using the Scherer equation from the XRD spectrum were found to be 20.5 and 11.2 nm, respectively. The XRD signals of EuO, Eu₂O₃, and Eu₂Se₃ were not observed in Figure 2a and b. However, we observed the signals at around 20 and 30 degrees that were not assigned to EuSe signals. The signal at around 30° is similar to that of EuSe₂ (30.18°) (Supporting Information Figure S1). We propose that the small EuSe₂ particles might be formed on the surface of Eu₁₋ₓSe **2**. We also observed that the XRD spectrum of organic Se ligands, (PPh₄)(Se₂P(C₆H₅)₂, gave the signals at around 20° in Figure 2c and Supporting Information Figure S2. Imperceptible shifts of the signals at around 20° might be due to transformation to different chemical structures by thermal reduction. By additional mass analysis, we also observed one of the different chemical structures, transformed Se-ligands (Supporting Information Figure S3). From those results, Eu₁₋ₓSe nanoparticles **2** would contain not only defects of Eu(II) but also the presence of EuSe₂ particles and organic Se compounds on the Eu₁₋ₓSe surface.

Typical TEM images of EuSe nanoparticles **1** are shown in Figure 3a and b. Cubic-shaped images with clear lattice fringes were observed, and their electron diffraction pattern was found to be good agreement with the isometric EuSe lattice (Supporting Information Figure S4). The image shows well-resolved lattice planes corresponding to the (200) plane of cubic EuSe. The aspect ratio between the long and short sides of the rectangular particles was evaluated for 300 nanoparticles and the average aspect ratio was about 1.1, indicating well-ordered cubic nanocrystals (Supporting Information Figure S5). The average crystal size evaluated by the TEM observations was found to be 23 nm (Figure 3c), and similar to the size measured by XRD (20.5 nm). Quantitative EDX analysis in the TEM measurements confirmed the stoichiometry of Eu₁₋ₓSe nanoparticles; Eu (42%):Se (58%) (Supporting Information Figure S6). The characteristic cubic shapes might be due to the NaCl-type fcc-structure of the EuSe lattice. As for the Eu₁₋ₓSe nanoparticles **2**, lots of Eu₁₋ₓSe nanoparticles stacked on the top of each other on the surface of the sample can be seen in Figure 3d and e. The average size of the stacked-Eu₁₋ₓSe nanoparticles evaluated
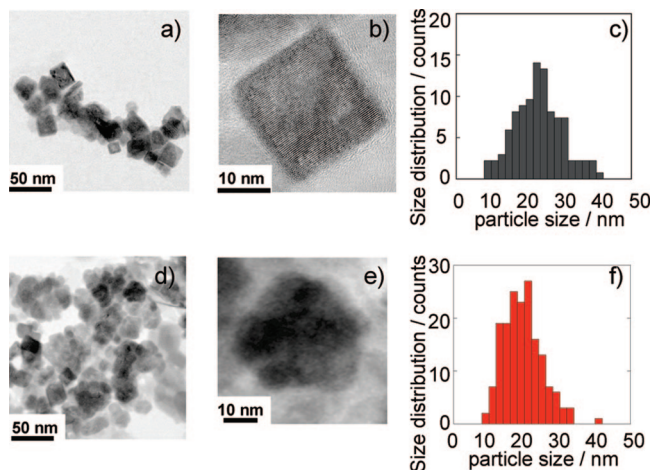
Figure 3. TEM images of $Eu_{1-x}Se$ nanoparticles: (a and b) high-resolution TEM images of $Eu_{1-x}Se$ nanoparticles **1**; (c) size distribution histogram of $Eu_{1-x}Se$ nanoparticles **1**; (d and e) high-resolution TEM images of $Eu_{1-x}Se$ nanoparticles **2**; (f) size distribution histogram of $Eu_{1-x}Se$ nanoparticles **2**.

for 171 nanoparticles was found to be 19.3 nm (Figure 3f: standard deviation = 5.5 nm). The EDX analysis in the TEM measurements showed a small number of Se atoms in the $Eu_{1-x}Se$ nanoparticles: Eu (22%):Se (78%) (Supporting Information Figure S7).

To explain about the EDX data, we estimated the atomic ratio concerned with ideal terrace and step model of EuSe lattice.[21] According to cubic-shaped $Eu_{1-x}Se$ **1**, total number f Eu and Se atoms in ideal EuSe nanocrystals (20.5 nm: terrace model) based on the lattice constant of EuSe (6.178 Å) was estimated to 146112. The EDX data ($Eu_{1-x}Se$ **1**: Eu, 0.41; Se, 0.58) indicates the presence of excess Se atoms (64146 atoms) on the $Eu_{1-x}Se$ surface. The percentage of excess amount of Se atoms in total Se atoms of $Eu_{1-x}Se$ **1** was found to be 30%. In contrast, an excess amount of Se atoms in $Eu_{1-x}Se$ **2** (11.2 nm: step model, Eu: 1296, Se: 1296) was estimated to be 3298 atoms. The percentage of excess amount of Se atoms in total Se atoms of $Eu_{1-x}Se$ **2** was found to be 72%. The difference between Figure 2a and 2b would be based on not only particle size but also excess percentage of Se compounds. From our estimations, we propose that the excess amount of Se atoms in $Eu_{1-x}Se$ nanoparticles **2** come from not only Eu defects but also presence of organic and inorganic Se compounds on the $Eu_{1-x}Se$ surface. Postulated preparative mechanisms of $Eu_{1-x}Se$ nanoparticles **1** and **2** are shown in Figure 4. Initial reaction conditions produce Eu(II) ions and ·$Se_2P(C_6H_5)_2$ through the electron transfer from the ligand to Eu(III). The ·$SeP(C_6H_5)_2$ moiety generates Se^{2-} and ·$SeP(C_6H_5)_2$. The reaction mechanism is similar to that of EuS nanoparticles obtained from single source precursor; $(PPh_4)[Eu(Et_2dtc)_4]·2H_2O$.[19] Thus, The $Eu_{1-x}Se$ nanoparticles seems to be formed by the reaction of Eu(II) with Se^{2-}, followed by particle growth. It is also proposed that the presence of tetraphenylphosinum cation ($P(C_6H_5)_4^+$) during the growth process has a pronounced effect on the shape and size of particles. $P(C_6H_5)_4^+$ cations easily stack on the anion species of the nanocrystals, that is, Se^{2-} anion sites.[19] The presence of $P(C_6H_5)_4^+$ stacked on $Eu_{1-x}Se$ nanoparticles **2** were confirmed by IR spectrum (Supporting Information Figure S8). A large

amount of Eu defects in $Eu_{1-x}Se$ nanoparticles **2** might be neutralized by $P(C_6H_5)_4^+$ on the surface. Formation of the stacked structure between $P(C_6H_5)_4^+$ on the particle surface would prevent particle growth and approach of Eu(II) ions to the particle surface. To estimate the amount of the organic compounds on the surface, we carried out the measurements of MIP-AES in addition to EDX analysis. The weight ratio of organic compounds in $Eu_{1-x}Se$ nanoparticles **1** and **2** (using MIP-AES and EDX analyses) were estimated to be about 30% and 45%, respectively (Table 1). The difference between the ratio percentages of organic compounds might be due to the presence of cationic $P(C_6H_5)_4^+$ stacked on the $Eu_{1-x}Se$ nanoparticles **2** and formation of organic Se compounds. We suggest that $P(C_6H_5)_4^+$ is one of the key compounds for control of particle size and shape and surface conditions.

Magentic Properties. Magnetic measurements of $Eu_{1-x}Se$ nanoparticles **1** and **2** were performed using a SQUID measurement. The temperature dependence of the magnetic susceptibility of $Eu_{1-x}Se$ nanoparticles **1** is shown in Figure 5a. We found that $Eu_{1-x}Se$ nanoparticles **1** displayed antiferromagnetic behavior (Néel point: T_N = 4.6 K). This Néel point of $Eu_{1-x}Se$ nanoparticles **1** agrees with that of bulk EuSe.[22] $Eu_{1-x}Se$ nanoparticles **2** also showed antiferromagnetic behavior, and their Néel point was estimated to be 4.1 K (Table 1). The saturation magnetization of $Eu_{1-x}Se$ nanoparticles **1** and **2** normalized by concentration of $Eu_{1-x}Se$ at 1.8 K was found to be 4.6 and 1.8 μB, respectively (Figure 5b). This value is much similar to that of corresponding EuS nanoparticles (saturation magnetization of EuS (paricle size: 36 nm) = 4.2 μB, saturation magnetization of EuS (paricle size: 21nm) = 2.6 μB).[17] The saturation magnetization of $Eu_{1-x}Se$ nanoparticles were smaller than the expected value of 7.0 μB for the $^8S_{7/2}$ state of Eu(II) at 0 K. In the particles range of 10–100 nm, ferromagnetic and antiferromagnetic nanoparticles are usually composed of a single domain structure.[23] The scale of 11 and 20 nm are probably effective in creating single domain structures in the $Eu_{1-x}Se$ nanoparticles. However, the complicated morphology of the $Eu_{1-x}Se$ nanoparticles was considered to affect the magnetic moment value, because the disorderly arrangement of tiny crystals on the surface of the nanoparticles possibly decrease the exchange interaction between Eu(II) ions. Especially, a smaller saturation magnetization of $Eu_{1-x}Se$ nanoparticles **2** might be due to the decrease of their crystal grain size, presence of the Eu defects, and formation of other Eu compounds such as $EuSe_2$.[17]

From the slope of the temperature versus $1/\chi$ asymptote of $Eu_{1-x}Se$ nanoparticles **1** and **2** ($3k_B/[Nm_B^2p^2]$: N = atom number, m_B = Bohr constant, k_B = Boltzmann constant), we calculated the experimental effective numbers of Bohr magneton (p) for the $Eu_{1-x}Se$ nanoparticles. The experimental effective number of Bohr magneton for the $Eu_{1-x}Se$ nanoparticles **1** and **2** was found to be 5.58 and 4.30, respectively (Figure 5a inset). Note that the $Eu_{1-x}Se$ nanoparticles **1** and **2** are composed by organic compounds (Table 1). The percentages of inorganic Eu compounds in $Eu_{1-x}Se$ nanoparticles **1** and **2** by using MIP-AES and EDX analyses are estimated to be 70% and 65%, respectively. With those estimations, the effective number of Bohr magneton for inorganic Eu compounds in $Eu_{1-x}Se$ nanoparticles **1** and **2** are found to be 7.97 and 6.61, respectively. The

(21) Hosokawa, H.; Fujiwara, H.; Murakoshi, K.; Wada, Y.; Yanagida, S.; Satoh, M. *J. Phys. Chem.* **1996**, *100*, 6649.

(22) Kasuya, T.; Yanase, A. *Rev. Modern Phys.* **1968**, *40*, 684.

(23) (a) Kittel, C. *Phys. Rev.* **1946**, *70*, 965. (b) Tomomura, A.; Matsuda, T.; Endo, J.; Arii, T.; Mihama, K. *Phys. Rev. Lett.* **1980**, *44*, 1430.
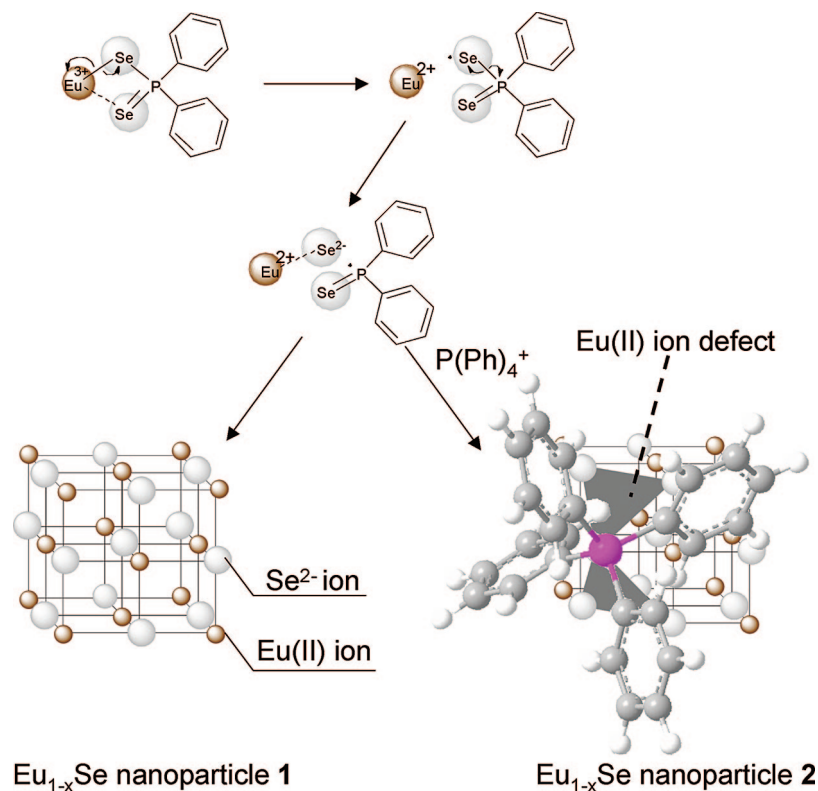
Figure 4. Postulated crystal growth mechanism of $Eu_{1-x}Se$ nanoparticles **1** and **2**.

Table 1. Magnetic and Magnetic-Optical Propreties of EuSe Nanoparticles **1** and **2**

	EuSe nanoparticles **1**	EuSe nanoparticles **2**
crystal grain size[a]	20.5 nm	11.2 nm
Néel point: T_N	4.6 K	4.1 K
effective number of Bohr magneton	5.58	4.30
organic compound weight ratio[b]	30%	45%
energy gap	1.8 eV	2.0 eV
Veldet constant[c]	2.1×10^{-3} deg/cm Oe	2.4×10^{-3} deg/cm Oe

[a] Calculated by the Scherer equation from XRD spectrum. [b] Estimated by using MIP-AES and EDX analyses. [c] Measured by Faraday rotation of polymer thin films containing EuSe nanoparticles at room temperature (concentration: 1 w %).
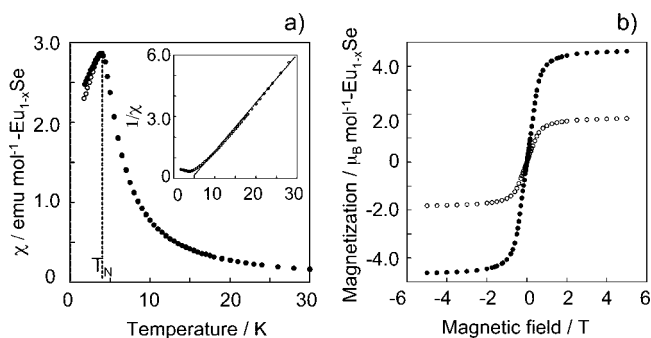

Figure 5. (a) Temperature dependence of χ and $1/\chi$ (inset) of $Eu_{1-x}Se$ nanoparticles **1** under field-cooled condition (●) and zero-field-cooled condition (○) at 0.1 T. (b) Magnetic field dependences of $Eu_{1-x}Se$ nanoparciles **1** (●) and **2** (○) at 1.8 K.

theoretical effective number of Bohr magneton for Eu(II) ($p = g[J(J + 1)]^{1/2}$: total angular momentum $J = ^7/_2$, gyromagnetic ratio $g \approx 2$) is calculated to be 7.94. Thus, the experimental p

for $Eu_{1-x}Se$ nanoparticles **1** agrees well with the theoretical p for the $4f^7$ configuration (Eu(II)). In a previous paper, we reported that smaller europium chalcogenide (EuO nanoparticles: average size = 3.4 nm) gave the ideal theoretical effective number of Bohr magneton ($p = 7.94$).[13a] These results indicate that $Eu_{1-x}Se$ nanoparticles **1** were constructed by Eu(II) ions. However, the saturation magnetization of $Eu_{1-x}Se$ nanoparticles **1** by concentration of $Eu_{1-x}Se$ at 1.8 K was found to be 4.6 μB, which is smaller than that of the $^8S_{7/2}$ state of Eu(II) at 0 K (7 μB). We propose that morphology of the $Eu_{1-x}Se$ nanoparticles **1** are affected by the disorderly arrangement of tiny Eu(II) compounds on the surface of the nanoparticles **1**.

In contrast, the experimental effective number of Bohr magneton of $Eu_{1-x}Se$ nanoparticles **2** was smaller than the theoretical effective number of Bohr magneton of Eu(II). In light of the previous finding, the estimated result of $Eu_{1-x}Se$ nanoparticles **2** may be due to their characteristic spin structure interacted by cationic $P(C_6H_5)_4^+$ and inorganic Eu compounds such as a $EuSe_2$ on the surface. We consider that there is a large amount of cationic $P(C_6H_5)_4^+$ and inorganic Eu compounds on the $Eu_{1-x}Se$ nanoparticles **2**, which might affect the spin structure of the $Eu_{1-x}Se$ nanoparticles **2**.

Magneto-Optical Properties. The magneto-optical properties of $Eu_{1-x}Se$ nanoparticles **1** and **2** were measured in poly(methylmethacrylate) (PMMA) thin films, prepared in accordance with a previously reported method.[15] The absorption spectra of the PMMA thin films containing $Eu_{1-x}Se$ nanoparticles **1** and **2** (PMMA-EuSe **1** and PMMA-EuSe **2**) are shown in Figure 6a. The 4f−5d ($4f_7(^8S_{7/2}) \rightarrow 4f_6(^7F_J)5d(t_{2g}, e_g)$) transitions of $Eu_{1-x}Se$ nanoparticles **1** and **2** were observed from 450 to 550 nm. We also measured the wavelength dependence of the Faraday rotation angle of PMMA-EuSe **1** and PMMA-EuSe **2** at room temperature (Figure 5b). The Faraday spectrum showed a clear positive and negative peak, which can be contributed to
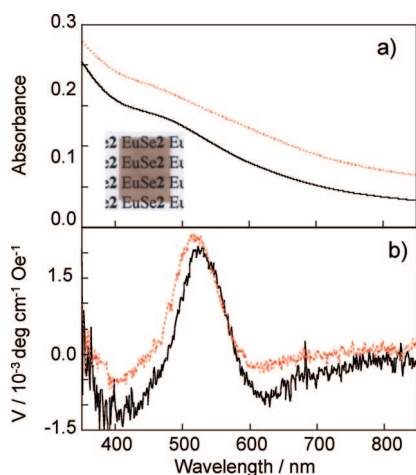
Figure 6. (a) Absorption and (b) Faraday rotation spectra of polymer thin films containing $Eu_{1-x}Se$ nanoparticles **1** (PMMA-EuSe **1**: solid line) and **2** (PMMA-EuSe **2**: dash line). Concentration of $Eu_{1-x}Se$ nanoaprticles in polymer films: 1 wt %. Inset picture shows PMMA-EuSe **2** (thickness: 4 μm).

the 4f−5d transitions of the EuSe nanoparticles. Their spectral shapes are very similar to that reported for bulk EuSe in the previous literature.[19] In particular, the wavelength of the positive peaks of PMMA-EuSe **1** and PMMA-EuSe **2** were successfully observed at 523 and 518 nm, respectively (Figure 1 and Table 1). The wavelength of their Faraday rotation peaks is the shortest in magneto-optic materials using europium chalcogenide. The energy gaps estimated by the thresholds of Faraday rotation spectra (720 and 650 nm) of **1** and **2** were found to be 1.8 and 2.0 eV, respectively. It clearly shows that PMMA-EuSe **2** is blue-shifted in comparison with **1** and bulk EuSe crystals (1.8 eV).[9] The level of the conduction band constructed from 5d orbitals would be affected by the surface cationic compounds through the surface coordination effects.[22] The Verdet constants estimated by Faraday rotation angle ($V = \tilde{\theta}Hl$: $\tilde{\theta}$, Faraday rotation angle; H, external magnetic field; l, sample thickness) of PMMA-EuSe **1** and PMMA-EuSe **2** were found to be 2.1×10^{-3} and 2.4×10^{-3} deg/cm Oe, respectively (Figure 5 and Table 1).

We have also carried out calculations of concentration-normalized Verdet constants of PMMA-EuSe **1** and **2** for comparison with previous bulk EuSe crystals and PMMA-EuS. The density of PMMA, EuSe, and EuS are 1.2, 6.5, and 5.7 g/cm³, respectively. Organic compound on the EuSe nanoparticle surfaces (HDA and $P(C_6H_5)_4^+$) was found to about 1 g/cm³. The volume percentages (unit: cm³) of $Eu_{1-x}Se$ nanoparticles in PMMA-EuSe **1** and **2** (1 wt %) are estimated to be 0.13 and 0.10 vol %, respectively. Consideration of the volume parcentages of $Eu_{1-x}Se$ nanoparticles in PMMA gives large Veldet constants ($Eu_{1-x}Se$ nanoparticles **1**, 1.62 deg/cm Oe; $Eu_{1-x}Se$ nanoparticles **2**, 2.40 deg/cm Oe), which is larger than the Veldet constant of bulk EuSe (0.16 deg/cm Oe at room temperature).[24] The concentration-normalized Verdet constant of PMMA-EuSe **2** was larger than that of PMMA-EuSe **1**. For PMMA-EuS, we reported a Veldet constant of 5.0×10^{-3} deg/cm Oe (concentra-

tion of EuS nanoparticles: 5.3 wt %) at 650 nm.[15] The concentration-normalized Verdet constant of PMMA-EuSe **2** is 5.3 times larger than that of the PMMA-EuS film (0.45 deg/cm Oe).

The large Faraday effect of EuSe nanoparticles might be attributed to their characteristic spin structure.[25] According to the spin structure of EuSe, it has been shown that bulk EuSe shows a ferrimagnetic phase (NNS) at a low temperature (1.8 $< T <$ 4.6 K, $T_c = 4.6$ K).[26] The magnetic properties of EuSe is affected by the surrounding environment and changed to ferromagnetic phase (NNSS).[27] Note that the $Eu_{1-x}Se$ nanoparticles possess lots of Eu(II) ions on the surface which are capped by the organic (HDA and $P(C_6H_5)_4^+$) and inorganic compounds such as $EuSe_2$. We expect that effective magneto-optical properties of $Eu_{1-x}Se$ nanoparticles are largely dominated by the special ferromagnetic phase of Eu(II) ions on the surface. It is also proposed that the spin–spin interaction in the EuSe lattice is affected by the characteristic Eu(II) ions on the nanoparticle surface. Recently, Hsu reported that the surface anisotropy dominates the magneto-dynamics in the magnetic nanoparticles.[28] The surface-modification effect on the $Eu_{1-x}Se$ nanoparticles is considered to be an additional factor resulting in a large Faraday effect for the PMMA- $Eu_{1-x}Se$ system.

Conclusion

We observed an effective Faraday effect of PMMA thin films containing $Eu_{1-x}Se$ nanoparticles at around 500 nm. Furthermore, we also suggest that the tetrapheniyphosphine cations, $P(C_6H_5)_4^+$, affected the particle size, shape, Eu-defects, spin-structure, and the magneto-optical properties of EuSe nanoparticles. Since the energy gap between the 4f orbitals and the conduction band depends on the size of the $Eu_{1-x}Se$ nanoparticles, the resonance wavelength for Faraday effects of EuSe nanoparticles can be controlled. Quantum-sized EuSe nanoparticles (<10 nm) would lead to development of the optimum isolator or magneto-optical memory in the range of blue light such as a GaN laser. The size-controlled lanthanide nanoparticles with a wide energy gap are expected to open up pioneering fields in nanomaterials chemistry and magneto-optic science.

Supporting Information Available: Additional TEM images, XRD, EDX analysis, and IR data. This material is available free of charge via the Internet at http://pubs.acs.org.

JA710165M

(24) Suits, J. C.; Argyle, B. E. *J. Appl. Phys.* **1965**, *36*, 1251.

(25) Oka, Y. *J. Magn. Soc. Jpn.* **1993**, *17*, 869.
(26) Mauger, A.; Godart, C. *Phys. Rep.* **1986**, *141*, 52.
(27) Rumpf, K.; Granitzer, P.; Kellner, W.; Kirchschlager, R.; Janecek, S.; Pasher, H.; Krenn, H. *Acta Phys. Pol., A* **2004**, *105*, 621.
(28) Hsu, K. H.; Wu, J. H.; Huang, Y. Y.; Wang, L. Y.; Lee, H. Y.; Lin, J. G. *J. Appl. Phys.* **2005**, *97*, 114322.